Published in final edited form as:
Biomaterials. 2015 January ; 39: 85–94. doi:10.1016/j.biomaterials.2014.10.067.

Repair of Dense Connective Tissues via Biomaterial-Mediated Matrix Reprogramming of the Wound Interface

Feini Qu, B.S.E.[1,2,3,4], **Michael P. Pintauro**[1,2,3], **Joanne Haughan, Mag. Med. Vet**[4], **Elizabeth A. Henning, B.S**[1,3], **John L. Esterhai, M.D**[1,3], **Thomas P. Schaer, V.M.D**[4], **Robert L. Mauck, Ph.D**[1,2,3,*], and **Matthew B. Fisher, Ph.D**[1,3,*]

[1]McKay Orthopaedic Research Laboratory, Department of Orthopaedic Surgery, Perelman School of Medicine, University of Pennsylvania, Philadelphia, PA 19104, USA

[2]Department of Bioengineering, School of Engineering and Applied Science, University of Pennsylvania, Philadelphia, PA 19104, USA

[3]Translational Musculoskeletal Research Center, Philadelphia Veterans Administration Medical Center, Philadelphia, PA 19104, USA

[4]Comparative Orthopaedic Research Laboratory, New Bolton Center, School of Veterinary Medicine, University of Pennsylvania, Kennett Square, PA 19348, USA

Abstract

Repair of dense connective tissues in adults is limited by their intrinsic hypocellularity and is exacerbated by a dense extracellular matrix (ECM) that impedes cellular migration to and local proliferation at the wound site. Conversely, healing in fetal tissues occurs due in part to an environment conducive to cell mobility and division. Here, we investigated whether the application of a degradative enzyme, collagenase, could reprogram the adult wound margin to a more fetal-like state, and thus abrogate the biophysical impediments that hinder migration and proliferation. We tested this concept using the knee meniscus, a commonly injured structure for which few regenerative approaches exist. To focus delivery and degradation to the wound interface, we developed a system in which collagenase was stored inside poly(ethylene oxide) (PEO) electrospun nanofibers and released upon hydration. Through a series of *in vitro* and *in vivo* studies, our findings show that partial digestion of the wound interface improves repair by creating a more compliant and porous microenvironment that expedites cell migration to and/or proliferation at the wound margin. This innovative approach of targeted manipulation of the wound interface, focused on removing the naturally occurring barriers to adult tissue repair, may find widespread application in the treatment of injuries to a variety of dense connective tissues.

[*]*Co-Corresponding Authors***Address for Correspondence:** Matthew B. Fisher, Ph.D. Assistant Professor of Biomedical Engineering North Carolina State University 4208C Engineering Building III Raleigh, NC 27695 Phone: (919) 515-5242 mbfisher@ncsu.edu Robert L. Mauck, Ph.D. Associate Professor of Orthopaedic Surgery and Bioengineering McKay Orthopaedic Research Laboratory Perelman School of Medicine University of Pennsylvania 36th Street and Hamilton Walk Philadelphia, PA 19104 Phone: (215) 898-3294 Fax: (215) 573-2133 lemauck@mail.med.upenn.edu.

Keywords

connective tissue; drug delivery; ECM (extracellular matrix); in vivo test; scaffold; wound healing

INTRODUCTION

Dense connective tissues play central load-bearing roles in the musculoskeletal system and thus are commonly injured. Damage to the knee and temporomandibular menisci [1], the annulus fibrosus of the intervertebral disc [2], and tendons and ligaments [3], alters joint biomechanics and instigates degenerative changes. The poor intrinsic healing capacity of these tissues, especially those lacking robust vasculature, reduces the efficacy of surgical repair procedures. Indeed, repair is so limited in some of these tissues that excision, rather than repair, is the treatment of choice [1]. Methods that improve endogenous repair would represent a significant advance in the treatment of injuries involving these tissues.

It is well appreciated that adult dense connective tissues have impaired healing compared to fetal tissues [4-7]. This decrease in healing potential is independent of the fetal biochemical milieu, in that differences persist in *in vitro* models [4, 5] as well as when fetal tissues are transplanted to the adult *in vivo* environment [7]. Instead, the biophysical properties of these tissues may dictate repair potential. Since repair and integration rely on the *de novo* synthesis of extracellular matrix (ECM) proteins to bridge the wound gap, it follows that access to the wound site and colonization by matrix-producing cells is essential for repair to occur. In fetal tissue, collagen fibers are slender and immature and the matrix is hypercellular relative to the adult. As tissues adapt to muscular contractions *in utero* and ambulation after birth, collagen fiber size and density increase, boosting mechanical properties, while cellularity markedly decreases [4, 8, 9]. While enabling function in adults, this high ECM density and stiffness, coupled with a lower cellularity, may pose barriers to endogenous healing. In contrast to 2D migration, cells in 3D must overcome the biophysical resistance of their microenvironment in order to move, including the high matrix stiffness [10] and limited pore size [11]. Similarly, tissue density and steric constraints may limit the capacity for local proliferative response. As tissue cellularity decreases, the distance a cell must travel also increases. Therefore, improving interstitial cell mobility through the dense ECM of adult tissues as well as the local proliferative potential may be a crucial first step to fostering repair and regeneration.

In this study, we use the knee meniscus as a test bed in which to evaluate a novel approach to enhance connective tissue repair. The meniscus is a fibrocartilaginous structure in the knee that mediates force transfer from the femur to the tibia. Meniscal ECM structure is intrinsic to its function, where circumferential collagen bundles develop to resist tensile hoop stresses [12, 13]. Tissue maturation is inversely related to the healing capacity of the meniscus, such that increasing patient age is correlated with worse clinical outcomes, including higher rates of repair failure [14, 15]. Importantly, patients over 40 with meniscal tears have fewer cells at the wound interface than younger patients [16]. Since 2D migration is comparable between fetal and adult meniscal fibrochondrocytes [4], these results suggest

that the 3D microenvironment engendered by tissue maturation antagonizes cellular migration, predisposing the meniscus to a limited repair capacity.

To evaluate the role of the ECM in meniscal healing, we reprogrammed the wound margin of the adult meniscus towards a 'fetal-like' state that would be more permissive to cell migration and division. Specifically, we tested whether treatment with collagenase, a matrix-degrading enzyme, could alter the density and stiffness of the wound microenvironment to expedite cellular egress from tissue and/or local proliferation so as to increase interfacial cellularity. To localize enzyme release, we developed composite electrospun nanofibrous networks that could be tuned to release collagenase upon implantation. Finally, we demonstrated enhanced repair using these novel materials in both a subcutaneous xenotransplant (rat) model and an orthotopic meniscal injury (ovine) model. These findings define a new paradigm in the treatment of connective tissue injuries, wherein the ECM at the wound interface can be reprogrammed to a state that is more amenable to repair.

MATERIALS AND METHODS

Evaluation of Cellular Egress from Meniscal Explants with Digestion

Menisci were isolated from adult cows (skeletally mature, ≤ 30 months) and tissue cylinders excised using an 8 mm biopsy punch. Cylinders were concentrically cored with a 4 mm punch to generate annuli and cores. To determine the effect of partial enzymatic digestion on cell egress from explants, annular samples were incubated in basal media (BM) [17] supplemented with collagenase (type IV from *Clostridium histolyticum*, ≥125 collagenase digestion units/mg solid; Sigma-Aldrich, St. Louis, MO) at 37°C for 3 hours on an orbital shaker, after which they were rinsed in 1X phosphate buffered saline (PBS). Three conditions were tested: BM only (Control), low-dose collagenase (LowC; 0.02 mg/mL), and high-dose collagenase (HighC; 0.06 mg/mL). Annuli were cultured at 37°C in BM (n = 3 samples/group). Cell egress was monitored on a daily basis via bright-field microscopy. After 10 days, explants were removed, embedded in optimal cutting temperature (OCT) sectioning medium, and cryosectioned axially to 16 μm thickness [17]. Sections were stained with Alcian Blue (AB) or Picrosirius Red (PSR) for sulfated proteoglycans (PGs) and collagen, respectively, and imaged under bright-field microscopy. The remaining adherent cells were incubated for 20 minutes with Hoechst 33342 (5 μg/mL; Invitrogen, Grand Island, NY) to label cell nuclei and imaged by fluorescence microscopy. Cell density from four distinct regions per sample was determined using ImageJ (Wayne Rasband, NIH).

Evaluation of Integration of Meniscal Repair Constructs with Digestion

To study the effect of enzymatic pre-treatment on integration, annuli and cores were incubated in BM with 0 (Control), 0.01 (LowC), or 0.05 mg/mL (HighC) collagenase at 37°C for 6 hours on an orbital shaker, rinsed with 1X PBS, and assembled into repair constructs [17]. Constructs were cultured in chemically-defined medium with 10 ng/mL TGF-β3 [17] for 1, 4, or 8 weeks. At set intervals, repair constructs were fixed in 4% paraformaldehyde, embedded in paraffin, and axially sectioned to 8 μm thickness for imaging, or embedded in OCT medium and axially sectioned to 20 μm thickness for micromechanical measurements. Second harmonic generation (SHG) imaging of the wound

interface was performed at an excitation wavelength of 840 nm (Carl Zeiss Microscopy GmbH, Jena, Germany) using unstained paraffin sections to visualize the fibrillar architecture of collagen at the earliest time point (1 week of *in vitro* culture). To identify nuclei, paraffin sections were stained with 4',6-diamidino-2-phenylindole (DAPI; Invitrogen) and imaged by fluorescence microscopy. Cell density at the interface was determined by counting the number of nuclei within 100 μm of the interface present in either the annulus or core (n = 4 samples/group) [17].

Evaluation of Tissue Micromechanics in Meniscal Repair Constructs with Digestion

Force spectroscopy was performed on cryosections in PBS using an atomic force microscope (AFM) mounted on top of an inverted optical microscope (Agilent, Santa Clara, California). A V-shaped pyramidal-tipped cantilever was positioned either at the tissue center or edge (a region within 100 μm of the wound interface). The probe tip was brought into contact and force and displacement recorded. Elastic moduli were computed using a Hertzian model [18] to an indentation depth of 300 nm using a custom program. Measurements with a fitted R^2 >= 0.98 were included (n = 3 samples/group, n = 10 measurements/sample).

Fabrication of Composite Nanofibrous Scaffolds to Enable Localized Digestion

Nanofibrous composites were formed via electrospinning using a custom tri-jet device [19]. Composites contained a poly(ε-caprolactone) (PCL; 80 kDa, Sigma-Aldrich) structural fiber fraction along with two water-soluble poly(ethylene oxide) (PEO; 200 kDa, Polysciences, Warrington, PA) fiber fractions. PEO fibers contained either no collagenase (Scaffold) or 15.6% type IV collagenase by mass (Scaffold+C) [17]. Electrospun mats were ~0.5 mm thick and stored at −20°C until use. To demonstrate collagenase activity, cylindrical juvenile articular cartilage samples were isolated using 4 mm biopsy punches. Cartilage cylinders were incubated in BM that contained either no scaffold (Control), a control scaffold (Scaffold, 0.04 mg), or a collagenase-releasing scaffold (Scaffold+C, 0.04 mg) at 37°C for 24 or 72 hours on an orbital shaker. Samples were cryotomed to 16 μm, stained with AB, and imaged [17].

Subcutaneous Assessment of Collagenase-Releasing Scaffolds

To test the effect of enzymatic treatment on meniscal repair *in vivo*, a nude rat xenotransplant model was employed. All procedures were approved by the Institutional Animal Care and Use Committee (IACUC) of the Philadelphia Veterans Affairs Medical Center. Adult bovine meniscal explants (8 mm diameter, 4 mm height) were incised to create a horizontal defect. The defect was either incubated in BM (Control) or in BM with 0.4 mg/mL collagenase at 37°C for 6 hours on an orbital shaker (aqC), or fille d with a control scaffold (Scaffold) or a collagenase-releasing scaffold (Scaffold+C). Scaffolds were cut to 5 x 5 mm with a 2 mm diameter fenestration to permit tissue-to-tissue and sterilized by UV. Defects were closed with absorbable sutures (3-0 Monocryl) before subcutaneous implantation into male athymic nude rats under aseptic conditions (Hsd:RH-*Foxn1*^{rnu}, ~300 g). Under general anesthesia, four pockets were created in each rat. One randomized construct per group was placed in each pocket and the incision was closed. At 1 week (n = 1/

group) and 4 weeks (n = 4/group), rats were euthanized by CO_2 asphyxiation. Retrieved samples were paraffin embedded, sectioned to 8 μm, and stained with Hemotoxylin & Eosin (H&E), PSR, or DAPI. Integration was quantified by dividing the cumulative length of integrated segments by the defect length in PSR sections (n = 3-4 samples/group). Given the increased cell density in *in vivo* samples, cellularity at the interface was evaluated using a modified protocol. Specifically, the nuclear signal from DAPI-stained micrographs was converted to white (intensity = 255) and background to black (intensity = 0) using ImageJ. Next, pixel intensity relative to the interface was averaged across the defect length, starting from the interface up to a distance 700 μm perpendicular to the defect. Signal intensity with respect to location was binned into 100 μm intervals for analysis (n = 4 samples/group). Finally, immunohistochemistry was performed to identify type I or type II collagen [20].

Assessment of Collagenase-Releasing Scaffolds in an Ovine Meniscal Repair Model

All procedures were approved by the IACUC at the University of Pennsylvania, and studies were performed in accordance with the NIH guidelines for the care and use of laboratory animals. Under general anesthesia, bilateral femorotibial joint surgeries were performed on five adult female Dorsett-Finn sheep. Following aseptic preparation, the medial collateral ligament (MCL) was isolated and reflected distally using a bone block to preserve the bone-ligament interface. A medial arthrotomy was performed followed by placement of stay sutures in the body of the medial meniscus to allow traction for increased exposure. A 10 mm full thickness longitudinal cut was made in the avascular zone of the meniscus using a scalpel blade, followed by repair with vertical mattress stitches using a braided polyester suture (2-0 Ethibond). Four groups were compared: 1) repair only, 2) treatment with a control PCL/PEO scaffold placed in the defect (trimmed to 10 mm in length x 3 mm in width, with three 1 mm diameter fenestrations along the length) in combination with repair, 3) treatment with a PCL/PEO scaffold releasing collagenase in combination with repair, and 4) a partial meniscectomy (removing the meniscus tissue axial to the longitudinal injury). Treatments were randomized (n = 3 for scaffold only group, n = 2 for all other groups). Afterwards, the joint capsule was repaired and the bone block was repositioned and secured using a bone screw and washer. Animals received a course of perioperative antimicrobials consisting of Potassium Penicillin and Gentamicin. Analgesia was provided in the form of transcutaneous fentanyl patches for 3 days, intra-articular morphine and bupivacaine delivered intra-operatively, and NSAIDs for 7 days. Animals were housed in individual 5 x 5 foot pens allowing for visual and olfactory contact. All animals had uneventful recoveries with no noticeable gait deficits after 2 weeks. At 4 weeks, sheep were sedated and euthanized with an injection of commercial euthanasia solution.

Following euthanasia, stifle joints were opened, and photographs taken of the meniscus, cartilage, and other soft tissues. Menisci and other soft tissues (e.g. ligaments, fat pad, etc.) were isolated and fixed in 10% formalin. Gross damage to the cartilage surfaces of the tibial plateau and femoral condyles was assessed via India ink staining as previously described [21] and quantified using ImageJ, where damage was expressed as a percentage of the total area of the cartilage surface. For histology, menisci, cartilage, and bone were paraffin embedded and sectioned to 6 μm thickness [20]. For the menisci, radial cross-sections through the injury site were stained with H&E and PSR and imaged. The cartilage and bone

sections were stained with Safranin O and Fast Green and imaged to visualize PGs and fibrous tissue, respectively.

Statistical Analysis

Statistical analyses were done using SYSTAT (Systat Software, Inc., San Jose, CA) and SPSS Statistics (IBM Corporation, Armonk, NY). Normality was assessed via the Kolmogorov-Smirnov test. One or two-way ANOVA with Tukey's HSD post hoc test were utilized to determine significant differences between groups ($p \leq 0.05$). Data is presented as the mean ± standard deviation, unless specified otherwise.

RESULTS

Partial enzymatic digestion enhances cellular egress from meniscal explants

Adult meniscal explants incubated in collagenase showed a dose-dependent degradation of collagen and removal of sulfated proteoglycans (PGs) at the tissue margin, indicated by Picrosirius Red (PSR) and Alcian Blue (AB) staining, respectively. While matrix digestion was minimal for the low-dose collagenase group (LowC), high-dose collagenase treatment (HighC) resulted in noticeable loss of peripheral matrix (**Fig. 1A**), consistent with previous findings [17]. When treated explants were placed on tissue culture substrates (**Fig. 1B**), meniscal fibrochondrocytes emerged within 6 days. At 10 days, cell outgrowth was higher for HighC samples (94 ± 43 cells/mm^2) compared to other groups, with a 36% and 395% increase over LowC (69 ± 60 cells/mm^2) and untreated control (19 ± 13 cells/mm^2) groups, respectively (**Fig. 1C**, $p \leq 0.05$). These data illustrate that the removal of physical impediments at the wound edge can expedite cellular egress.

Degradation of the wound interface reduces matrix density, increases cellularity, and alters micromechanics

To focus on the wound interface, partial digestion of annuli and cores was performed prior to their reassembly into concentric 'repair' constructs. Collagenase pre-treatment resulted in dose-dependent modulation of the wound interface. After 1 week, second harmonic generation (SHG) imaging revealed dense collagen bundles in untreated controls, with no tissue formation across the wound gap. Conversely, HighC samples had thin, immature fibrils populated by a higher number of cells bridging the wound gap (**Figs. 2A & 2B**). Indeed, cell density at the annulus-core boundary was greater for HighC samples (444 ± 139 cells/mm^2) compared to all other groups by the 1 week time point, with a 96% and 242% increase over LowC (226 ± 62 cells/mm^2) and control (130 ± 37 cells/mm^2) groups, respectively (**Fig. 2C**, $p \leq 0.05$). These differences in matrix density, defect integration, and cellularity persisted through 8 weeks for HighC compared to all other groups, despite stable tissue-to-tissue apposition in all groups. Once the differences in cell density were established, these values did not change with additional time in culture, suggesting that partial degradation leads to a rapid and sustainable accumulation of cells at the wound margin.

Force spectroscopy via atomic force microscopy (AFM) of repair constructs (**Fig. 3A**) cultured for 8 weeks revealed persistent changes in micromechanics at the interface with

treatment (**Fig. 3B**). The Young's modulus (E_Y) of the defect edge for LowC (345 ± 138 kPa) and HighC (210 ± 79 kPa) samples were lower than that of controls (488 ± 155 kPa) (**Fig. 3C**, $p \leq 0.05$). Digestion with high-dose collagenase also reduced E_Y of the HighC construct center (312 ± 133 kPa) compared to that of LowC (441 ± 151 kPa) and control (496 ± 120 kPa) groups. Taken together, our results suggest that collagenase dose can be tuned to mediate local matrix digestion and advance repair.

Composite Scaffolds Releasing Collagenase Improve Integration in a Subcutaneous Model

Given the improvements in repair observed *in vitro* with collagenase pre-treatment, we next translated these findings to the *in vivo* scenario. Here, we utilized a multi-jet electrospinning setup in which poly(ε-caprolactone) (PCL) fibers (stable, structural) were electrospun along with two poly(ethylene oxide) (PEO) fiber fractions (soluble, factor delivering), with each fraction collected simultaneously onto a common rotating mandrel (**Fig. 4A**) [19]. This fabrication scheme resulted in an aligned composite scaffold containing ~50-60% PEO by mass, where the PEO fraction delivered collagenase at varying doses. The morphology and bioactivity of PCL and PEO nanofibers with or without collagenase have been previously characterized [17, 22]. Incubation of cartilage explants with collagenase-releasing scaffolds (Scaffold+C) (**Fig. 4B**) decreased AB staining intensity at the tissue edge within 24 hours (data not shown), with further reductions at 72 hours (**Fig. 4C**). Untreated explants (Control) or those incubated with non-bioactive scaffolds (Scaffold) did not show any alterations in staining intensity.

To evaluate scaffold-mediated repair in an *in vivo* setting, we placed bovine meniscal repair constructs, either pre-treated with aqueous collagenase (aqC) or provided with a bioactive scaffold (Scaffold+C), subcutaneously in nude rats (**Fig. 5A**). Empty defects (Control) and non-bioactive scaffolds (Scaffold) were used as negative controls. Control and Scaffold groups retained a dense local ECM, had few cells present at the wound margin, and showed little matrix deposition at the center of the defect. In contrast, samples pre-treated with aqC or with Scaffold+C showed increased cellularity and interface bridging by 1 week (data not shown). Quantification showed a trend towards improved integration for Scaffold+C samples (87 ± 9%) compared to controls (59 ± 16%) by 4 weeks (**Fig. 5B**, $p = 0.07$), with regions of the scaffold staining positive for cells (**Fig. 5C**) and types I and II collagen (**Fig. 5D**).

As seen with aqueous collagenase treatment *in vitro*, the increase in cellularity at the wound edge began as early as 1 week (data not shown). After 4 weeks, cell signal intensity local to the interface was higher in Scaffold+C repairs compared to all other groups **(Fig. 6A**). This increase in cell number was significant for a distance up to 300 μm from the wound compared to aqC, and 400 μm compared to Control and Scaffold groups (**Fig. 6B**, $p \leq 0.05$). The highest cell density was within 100 μm of the interface for both aqC and Scaffold+C groups. This gradient in cellularity was not observed in Control or Scaffold groups, where the matrix remained intact. Collectively, these data suggest that collagenase-releasing scaffolds can modulate repair *in vivo*.

Composite Scaffolds Releasing Collagenase Promote Meniscal Repair in an Ovine Model

To advance this technology toward clinical translation, we tested scaffolds in a pilot study using an orthotopic large animal representative of the mechanically challenging and avascular environment of the adult synovial joint. The ovine model was chosen based on its consistency with human meniscal anatomy, function, and limited healing response [23]. Full-thickness vertical incisional defects were created in the avascular body of the medial meniscus (**Fig. 7A**). Defects were repaired by suture following standard surgical protocol (Repair), or repaired with suture in addition to a control scaffold (Scaffold) or a scaffold releasing collagenase (Scaffold+C). One additional group consisted of a partial meniscectomy (partial removal). Four weeks post-operatively, all Scaffold and Scaffold+C groups and one Repair group remained intact. One Repair sample failed partially due to suture pulling through the injury site. Histological staining of the meniscus (**Fig. 7B**) revealed variations in healing based on group. For partial meniscectomy, the original injury site was readily visualized, with no new tissue formation. For the Repair group, the injury was clearly identified as a gap that persisted across the inner and outer portions of the meniscus, with no new tissue formation. Similar findings were obtained for the Scaffold group. Defects treated with Scaffold+C groups, however, showed clear apposition of the margins and tissue formation both within and around the scaffold across the length and height of the defect, suggestive of a robust healing response (**Fig. 7B, inset**).

To determine whether cartilage and other joint structures were perturbed by either injury or treatment, India ink staining was performed. This analysis revealed low levels (< 5%) for all specimens from the non-operative joint compartment (the lateral tibial plateau, **Fig. 7C**). In the operative compartment (the medial tibial plateau), the partial meniscectomy group had the highest values. All repair groups had low levels of cartilage damage (3-11%), though all were higher than that of the non-operative side. Evaluation of other joint tissues (anterior cruciate ligament, posterior cruciate ligament, fat pad, synovium) showed no changes with Scaffold or Scaffold+C compared to controls (data not shown), indicating that enzymatic degradation was indeed confined to the wound margin.

DISCUSSION

This study demonstrates that matrix reprogramming of the adult meniscal ECM to a fetal-like state improves integrative repair. This *in vivo* analysis, consistent with our previous *in vitro* studies [17], illustrates the potential of partial degradation of the meniscal wound edge to enhance healing. Here, we establish that delivery of collagenase facilitates repair by expediting cell migration to and/or proliferation at the wound site. Furthermore, we reduce this concept to practice by demonstrating that localized collagenase delivery via composite nanofibrous scaffolds *in vivo* enhances closure of meniscal defects without perturbing other intra-articular tissues. Collectively, these data define a novel methodology for the treatment of dense connective tissues that are recalcitrant to regenerative healing due to the intrinsic characteristics of their dense and hypocellular ECM.

This new endogenous tissue engineering approach may find widespread application in injuries to tissues having low cellularity or lacking proper blood supply. When circulating stem cells are precluded from the repair response (as is the case with dense connective

tissues), the pool of reparative cells is limited to those residing within the tissue itself or those that migrate from neighboring structures. Unlike the hypercellular repair response seen in injured fetal tissue (**Fig. 8A**), cells within adult tissue do not readily undergo interstitial migration or local proliferation, resulting in a hypocellular wound margin with minimal repair tissue formation (**Fig. 8B**). It is likely that the high density and stiffness of collagen bundles retard proteolysis-mediated migration and restrict proliferation [24]. To enhance cell mobility and provide sufficient space for division, we digested the tissue border with collagenase, a proteolytic enzyme that cleaves fibrillar collagens (**Fig. 8C**). Until recently, partial degradation has only been explored in the context of articular cartilage repair. Short-term enzymatic treatment can increase interfacial chondrocyte density and improve interfacial strength *in vitro* [25], as well as enhance integration of cartilage explants to engineered cartilage [26] and to acellular scaffolds [27]. In concordance with this literature, we show here that collagenase also enhances the integration of the knee meniscus, and can be applied in conjunction with a standard suture repair to meniscal injuries *in vivo*.

Reducing ECM stiffness and density at the wound margin via enzymatic treatment may improve fibrous wound healing by freeing cells from their spatial confinements to improve migration and/or local proliferation, although other factors may contribute as well. For instance, collagen fragments can act as biochemical signals for cell proliferation [28] and migration [29]. Likewise, exposing cells to the underlying collagen network via depletion of PGs may stimulate matrix deposition [30]. Degrading the defect edge may also release matrix-bound latent transforming growth factor-beta (TGF-β) [31], which could promote either a myofibroblastic phenotype that may be beneficial to fibrous wound healing [32, 33] and/or recruit endogenous stem cells to the wound environment [34]. Regardless of the precise mechanism of action, increasing the quantity of matrix-producing cells at the wound interface benefits the early phase of repair. While collagenase improved the interface in our study, additional cues may be required to accelerate ECM maturation to prevent re-injury. For example, delivery of TGF-β could enhance matrix synthesis [35], while lysyl oxidase could stabilize the wound interface by promoting collagen crosslinking [30]. On the tissue level, controlled resumption of load bearing activity, engendering both tensile and compressive loading, could promote development of native tissue architecture [36, 37]. Since 3D migration depends on deformation and contraction-mediated movement through tight interstitia, cell mechanics and contractility pathways might also be manipulated to enhance mobility [11, 38] and thereby improve endogenous tissue repair.

In order to translate our findings towards clinical application, we developed methods by which enzyme delivery could be localized to the wound margin. Injectable collagenase is currently in clinical use for the treatment of Dupuytren's contracture, a fibroproliferative disorder [39], where the factor is directly injected into the aberrant tissue. However, such diffuse, non-targeted injection into a synovial joint would reduce the efficacy of the factor and could damage surrounding intra-articular structures. To overcome this, we developed collagenase-releasing nanofibrous scaffolds that could be inserted into the wound site. We and others have used such bioactive nanofiber-based systems to direct new tissue formation for the meniscus and other musculoskeletal tissues [17, 40, 41]. Here, we took advantage of the rapid dissolution of the PEO fiber fraction to provide an immediate and localized burst

delivery of enzyme. Incubating these scaffolds with cartilage and meniscus resulted in matrix digestion and PG removal at the tissue margins, demonstrating retention of bioactivity during scaffold fabrication and sterilization. When inserted into meniscal defects, composite scaffolds released collagenase in a targeted manner, creating a gradient of matrix loss. After PEO dissolution, the stable, aligned PCL fiber fraction remained as a physical template to provide instruction for ECM synthesis [42]. Both PEO and PCL are FDA-approved materials, making these acellular scaffolds an attractive system for translation.

Having established a biocompatible delivery vehicle, we next evaluated whether biomaterial-mediated matrix degradation of the meniscal wound interface could be achieved *in vivo*, and whether this might enhance cellular infiltration, local proliferation, and tissue integration. In both a subcutaneous xenotransplant model in the nude rat and an orthotopic injury model in adult sheep, meniscal defects treated with collagenase-releasing scaffolds showed improved cellularity of the wound margin. While it is difficult to decouple increased migration at the wound margin from cell division, both may have contributed to increase local cellularity within this region; future studies will include BrdU labeling during repair to identify the specific contributions of these two complementary processes. Regardless, this increased cellularity at the wound margin correlated with matrix deposition around and within the scaffolds, resulting in wound closure by 4 weeks. Notably, there was neither gross nor histological evidence of adverse changes outside the defect. Based on this data, we believe that, when used alongside a standard suture repair, this acellular, bioactive scaffold will enable wound healing in an environment that is biologically and biomechanically unfavorable for repair.

While nanofibrous composites have previously been exploited for tissue engineering of the meniscus [42], this is the first instance where localized delivery of therapeutics via nanofibers was used to enhance endogenous meniscal integration. Simultaneous electrospinning of multiple, discrete fiber families allows for the fabrication of highly tunable scaffolds [19] that are capable of delivering multiple biologic factors with varying release profiles. As such, this technology may be modified to deliver additional agents to facilitate repair, including chemoattractants to recruit both native [43] and endogenous stem cells [44], growth factors to promote matrix deposition [30, 35], and anti-inflammatories to prevent matrix catabolism [45]. Likewise, the aligned nanofibers themselves can direct matrix deposition [46], allowing the scaffold topography to foster tissue formation that recapitulates essential structural and mechanical anisotropies of the native meniscus and other organized connective tissues, such as tendons and ligaments [47]. Lastly, biomaterial-mediated matrix reprogramming may be utilized to enhance the integration of autologous meniscal fragments [48] or bioengineered replacements [21, 49-51] to surrounding native tissue, currently a major logistical hurdle to translation.

CONCLUSIONS

In summary, limited cell mobility arising from inherent changes that occur with maturation may limit endogenous healing of the adult meniscus and other dense connective tissues. An innovative strategy to promote repair may be to first reduce the natural biophysical constraints on native cells so as to facilitate their migration to and local proliferation at the

wound site. Given the long time course and high re-failure rate of fibrous tissue repair, translational tools that enhance integration will improve treatment options for a multitude of common orthopaedic injuries, changing the paradigm from one of resection to one of regeneration.

ACKNOWLEDGEMENTS

We thank the staff at the Philadelphia VA Medical Center and the New Bolton Center for veterinary and administrative support. We also thank Claire McLeod and Brian Cosgrove for assistance with AFM. This work was supported by the National Institutes of Health (R01 AR056624, T32 GM007170, T32 AR007132), the Department of Veterans Affairs (I01 RX000174), the Musculoskeletal Transplant Foundation, the Armour-Lewis Foundation, and the School of Veterinary Medicine. The content is solely the responsibility of the authors and does not represent the official views of the National Institutes of Health or the Department of Veterans Affairs. No funding source had a role in the study design, collection, analysis and interpretation of data, writing of the manuscript, or the decision to submit the manuscript for publication.

REFERENCES

1. Makris EA, Hadidi P, Athanasiou KA. The knee meniscus: structure-function, pathophysiology, current repair techniques, and prospects for regeneration. Biomaterials. 2011; 32(30):7411–31. [PubMed: 21764438]
2. Guterl CC, See EY, Blanquer SB, Pandit A, Ferguson SJ, Benneker LM, et al. Challenges and strategies in the repair of ruptured annulus fibrosus. Eur Cell Mater. 2013; 25:1–21. [PubMed: 23283636]
3. Yang G, Rothrauff BB, Tuan RS. Tendon and ligament regeneration and repair: clinical relevance and developmental paradigm. Birth Defect Res C. 2013; 99(3):203–22.
4. Ionescu LC, Lee GC, Garcia GH, Zachry TL, Shah RP, Sennett BJ, et al. Maturation state-dependent alterations in meniscus integration: implications for scaffold design and tissue engineering. Tissue Eng Part A. 2011; 17(1-2):193–204. [PubMed: 20712419]
5. Stalling SS, Nicoll SB. Fetal ACL fibroblasts exhibit enhanced cellular properties compared with adults. Clin Orthop Relat Res. 2008; 466:3130–7. [PubMed: 18648900]
6. Beredjiklian PK, Favata M, Cartmell JS, Flanagan CL, Crombleholme TM, Soslowsky LJ. Regenerative versus reparative healing in tendon: a study of biomechanical and histological properties in fetal sheep. Ann Biomed Eng. 2003; 31(10):1143–52. [PubMed: 14649488]
7. Favata M, Beredjiklian PK, Zgonis MH, Beason DP, Crombleholme TM, Jawad AF, et al. Regenerative properties of fetal sheep tendon are not adversely affected by transplantation into an adult environment. J Orthop Res. 2006; 24(11):2124–2132. [PubMed: 16944473]
8. Clark CR, Ogden JA. Development of the menisci of the human knee joint. Morphological changes and their potential role in childhood meniscal injury. J Bone Joint Surg Am. 1983; 65(4):538–47. [PubMed: 6833331]
9. Ansorge HL, Adams S, Birk DE, Soslowsky LJ. Mechanical, compositional, and structural properties of the post-natal mouse Achilles tendon. Ann Biomed Eng. 2011; 39(7):1904–13. [PubMed: 21431455]
10. Ehrbar M, Sala A, Lienemann P, Ranga A, Mosiewicz K, Bittermann A, et al. Elucidating the role of matrix stiffness in 3D cell migration and remodeling. Biophys J. 2011; 100(2):284–93. [PubMed: 21244824]
11. Wolf K, Te Lindert M, Krause M, Alexander S, Te Riet J, Willis AL, et al. Physical limits of cell migration: control by ECM space and nuclear deformation and tuning by proteolysis and traction force. J Cell Biol. 2013; 201(7):1069–84. [PubMed: 23798731]
12. Shrive NG, O'Connor JJ, Goodfellow JW. Load-bearing in the knee joint. Clin Orthop Relat Res. 1978; 131:279–87. [PubMed: 657636]
13. Walker PS, Erkman MJ. The role of the menisci in force transmission across the knee. Clin Orthop Relat Res. 1975; 109:184–92. [PubMed: 1173360]

14. Eggli S, Wegmuller H, Kosina J, Huckell C, Jakob RP. Long-term results of arthroscopic meniscal repair. An analysis of isolated tears. Am J Sports Med. 1995; 23(6):715–20. [PubMed: 8600740]
15. Vanderhave KL, Moravek JE, Sekiya JK, Wojtys EM. Meniscus tears in the young athlete: results of arthroscopic repair. J Pediatr Orthop. 2011; 31(5):496–500. [PubMed: 21654455]
16. Mesiha M, Zurakowski D, Soriano J, Nielson JH, Zarins B, Murray MM. Pathologic characteristics of the torn human meniscus. Am J Sports Med. 2007; 35(1):103–12. [PubMed: 17092929]
17. Qu F, Lin JM, Esterhai JL, Fisher MB, Mauck RL. Biomaterial-mediated delivery of degradative enzymes to improve meniscus integration and repair. Acta Biomater. 2013; 9(5):6393–402. [PubMed: 23376132]
18. Sanchez-Adams J, Wilusz RE, Guilak F. Atomic force microscopy reveals regional variations in the micromechanical properties of the pericellular and extracellular matrices of the meniscus. J Orthop Res. 2013; 31(8):1218–25. [PubMed: 23568545]
19. Baker BM, Nerurkar NL, Burdick JA, Elliott DM, Mauck RL. Fabrication and modeling of dynamic multipolymer nanofibrous scaffolds. J Biomech Eng. 2009; 131(10):101012. [PubMed: 19831482]
20. Farrell MJ, Fisher MB, Huang AH, Shin JI, Farrell KM, Mauck RL. Functional properties of bone marrow-derived MSC-based engineered cartilage are unstable with very long-term in vitro culture. J Biomech. 2013; 47(9):2173–2182. [PubMed: 24239005]
21. Cook JL, Fox DB, Malaviya P, Tomlinson JL, Kuroki K, Cook CR, et al. Long-term outcome for large meniscal defects treated with small intestinal submucosa in a dog model. Am J Sports Med. 2006; 34(1):32–42. [PubMed: 16157845]
22. Baker BM, Gee AO, Metter RB, Nathan AS, Marklein RA, Burdick JA, et al. The potential to improve cell infiltration in composite fiber-aligned electrospun scaffolds by the selective removal of sacrificial fibers. Biomaterials. 2008; 29(15):2348–58. [PubMed: 18313138]
23. Arnoczky SP, Cook JL, Carter T, Turner AS. Translational models for studying meniscal repair and replacement: what they can and cannot tell us. Tissue Eng Part B. 2010; 16(1):31–9.
24. Bott K, Upton Z, Schrobback K, Ehrbar M, Hubbell JA, Lutolf MP, et al. The effect of matrix characteristics on fibroblast proliferation in 3D gels. Biomaterials. 2010; 31(32):8454–64. [PubMed: 20684983]
25. Van de Breevaart Bravenboer J, der Maur CD, Bos PK, Feenstra L, Verhaar JA, Weinans H, et al. Improved cartilage integration and interfacial strength after enzymatic treatment in a cartilage transplantation model. Arthritis Res Ther. 2004; 6(5):R469–76. [PubMed: 15380046]
26. Obradovic B, Martin I, Padera RF, Treppo S, Freed LE, Vunjak-Novakovic G. Integration of engineered cartilage. J Orthop Res. 2001; 19(6):1089–97. [PubMed: 11781010]
27. Ng KW, Wanivenhaus F, Chen T, Hsu HC, Allon AA, Abrams VD, et al. A novel macroporous polyvinyl alcohol scaffold promotes chondrocyte migration and interface formation in an in vitro cartilage defect model. Tissue Eng Part A. 2012; 18(11-12):1273–1281. [PubMed: 22435602]
28. Koohestani F, Braundmeier AG, Mahdian A, Seo J, Bi J, Nowak RA. Extracellular matrix collagen alters cell proliferation and cell cycle progression of human uterine leiomyoma smooth muscle cells. PloS one. 2013; 8(9):e75844. [PubMed: 24040420]
29. Shi L, Ermis R, Garcia A, Telgenhoff D, Aust D. Degradation of human collagen isoforms by Clostridium collagenase and the effects of degradation products on cell migration. Int Wound J. 2010; 7(2):87–95. [PubMed: 20529148]
30. Makris EA, MacBarb RF, Paschos NK, Hu JC, Athanasiou KA. Combined use of chondroitinase-ABC, TGF-beta1, and collagen crosslinking agent lysyl oxidase to engineer functional neotissues for fibrocartilage repair. Biomaterials. 2014; 35(25):6787–6796. [PubMed: 24840619]
31. Tatti O, Vehvilainen P, Lehti K, Keski-Oja J. MT1-MMP releases latent TGF-beta1 from endothelial cell extracellular matrix via proteolytic processing of LTBP-1. Exp Cell Res. 2008; 314(13):2501–14. [PubMed: 18602101]
32. Kambic HE, Futani H, McDevitt CA. Cell, matrix changes and alpha-smooth muscle actin expression in repair of the canine meniscus. Wound Repair Regen. 2000; 8(6):554–61. [PubMed: 11208183]
33. Hinz B. Formation and function of the myofibroblast during tissue repair. J Invest Dermatol. 2007; 127(3):526–37. [PubMed: 17299435]

34. Lee CH, Cook JL, Mendelson A, Moioli EK, Yao H, Mao JJ. Regeneration of the articular surface of the rabbit synovial joint by cell homing: a proof of concept study. Lancet. 2010; 376(9739): 440–8. [PubMed: 20692530]
35. Ionescu LC, Lee GC, Huang KL, Mauck RL. Growth factor supplementation improves native and engineered meniscus repair in vitro. Acta Biomater. 2012; 8(10):3687–94. [PubMed: 22698946]
36. Baker BM, Shah RP, Huang AH, Mauck RL. Dynamic tensile loading improves the functional properties of mesenchymal stem cell-laden nanofiber-based fibrocartilage. Tissue Eng Part A. 2011; 17(9-10):1445–55. [PubMed: 21247342]
37. Puetzer JL, Ballyns JJ, Bonassar LJ. The effect of the duration of mechanical stimulation and post-stimulation culture on the structure and properties of dynamically compressed tissue-engineered menisci. Tissue Eng Part A. 2012; 18(13-14):1365–75. [PubMed: 22429287]
38. Harada T, Swift J, Irianto J, Shin JW, Spinler KR, Athirasala A, et al. Nuclear lamin stiffness is a barrier to 3D migration, but softness can limit survival. J Cell Biol. 2014; 204(5):669–82. [PubMed: 24567359]
39. Bendon CL, Giele HP. Collagenase for Dupuytren's disease of the thumb. J Bone Joint Surg Br. 2012; 94(10):1390–2. [PubMed: 23015566]
40. Fu YC, Nie H, Ho ML, Wang CK, Wang CH. Optimized bone regeneration based on sustained release from three-dimensional fibrous PLGA/HAp composite scaffolds loaded with BMP-2. Biotechnol Bioeng. 2008; 99(4):996–1006. [PubMed: 17879301]
41. Manning CN, Schwartz AG, Liu W, Xie J, Havlioglu N, Sakiyama-Elbert SE, et al. Controlled delivery of mesenchymal stem cells and growth factors using a nanofiber scaffold for tendon repair. Acta Biomater. 2013; 9(6):6905–14. [PubMed: 23416576]
42. Baker BM, Shah RP, Silverstein AM, Esterhai JL, Burdick JA, Mauck RL. Sacrificial nanofibrous composites provide instruction without impediment and enable functional tissue formation. Proc Natl Acad Sci U S A. 2012; 109(35):14176–81. [PubMed: 22872864]
43. Bhargava MM, Attia ET, Murrell GA, Dolan MM, Warren RF, Hannafin JA. The effect of cytokines on the proliferation and migration of bovine meniscal cells. Am J Sports Med. 1999; 27(5):636–43. [PubMed: 10496583]
44. Barreto Henriksson H, Lindahl A, Skioldebrand E, Junevik K, Tangemo C, Mattsson J, et al. Similar cellular migration patterns from niches in intervertebral disc and in knee-joint regions detected by in situ labeling: an experimental study in the New Zealand white rabbit. Stem Cell Res Ther. 2013; 4(5):104. [PubMed: 24004687]
45. McNulty AL, Weinberg JB, Guilak F. Inhibition of matrix metalloproteinases enhances in vitro repair of the meniscus. Clin Orthop Relat Res. 2009; 467(6):1557–67. [PubMed: 18975039]
46. Baker BM, Mauck RL. The effect of nanofiber alignment on the maturation of engineered meniscus constructs. Biomaterials. 2007; 28(11):1967–77. [PubMed: 17250888]
47. Zhang X, Bogdanowicz D, Erisken C, Lee NM, Lu HH. Biomimetic scaffold design for functional and integrative tendon repair. J Shoulder Elbow Surg. 2012; 21(2):266–277. [PubMed: 22244070]
48. Kobayashi Y, Yasuda K, Kondo E, Katsura T, Tanabe Y, Kimura M, et al. Implantation of autogenous meniscal fragments wrapped with a fascia sheath enhances fibrocartilage regeneration in vivo in a large harvest site defect. Am J Sports Med. 2010; 38(4):740–8. [PubMed: 20139330]
49. Maher SA, Rodeo SA, Doty SB, Brophy R, Potter H, Foo LF, et al. Evaluation of a porous polyurethane scaffold in a partial meniscal defect ovine model. Arthroscopy. 2010; 26(11):1510–9. [PubMed: 20855181]
50. Verdonk R, Verdonk P, Huysse W, Forsyth R, Heinrichs EL. Tissue ingrowth after implantation of a novel, biodegradable polyurethane scaffold for treatment of partial meniscal lesions. Am J Sports Med. 2011; 39(4):774–82. [PubMed: 21383084]
51. Kon E, Filardo G, Zaffagnini S, Di Martino A, Di Matteo B, Marcheggiani Muccioli GM, et al. Biodegradable polyurethane meniscal scaffold for isolated partial lesions or as combined procedure for knees with multiple comorbidities: clinical results at 2 years. Knee Surg Sports Traumatol Arthrosc. 2014; 22(1):128–134. [PubMed: 23223879]

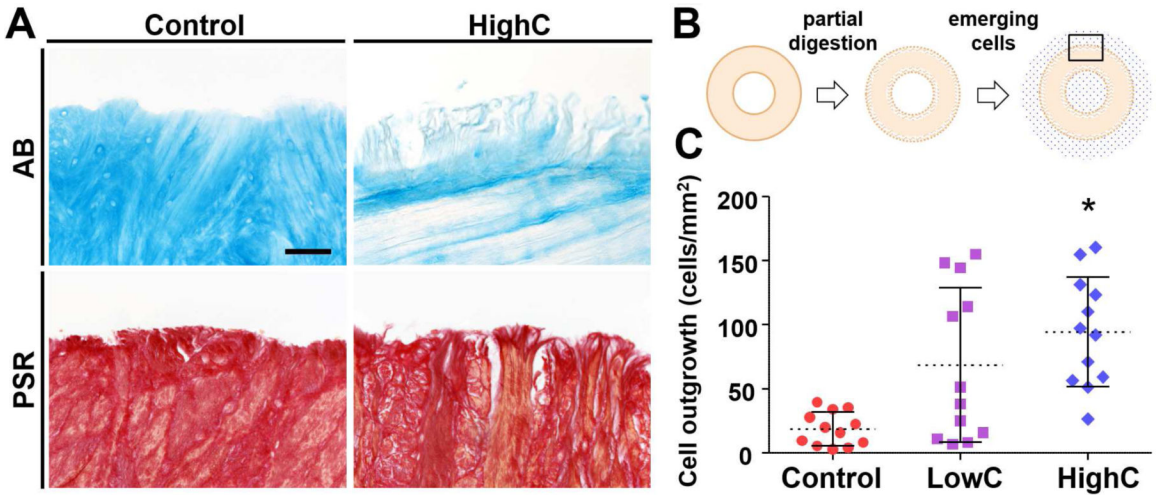

Figure 1. Partial enzymatic digestion with collagenase enhances cellular egress from meniscal explants *in vitro*

(A) Alcian Blue (AB) and Picrosirius Red (PSR) staining for proteoglycans (PGs) and collagen, respectively. Collagenase digestion removes PGs and collagens from the tissue edge. Scale = 100 μm. (B) Top-down schematic illustrating partial enzymatic digestion of ring-shaped explants and emergent cells (blue dots). Box indicates area imaged for Fig. 1A. (C) Cell outgrowth onto tissue culture-treated plates 10 days after pre-treatment with low- (LowC; 0.02 mg/mL) and high-dose (HighC; 0.06 mg/mL) collagenase (n = 3 samples/group, 4 measurements/sample, mean ± standard deviation). * = $p \leq 0.05$ vs. Control and LowC.

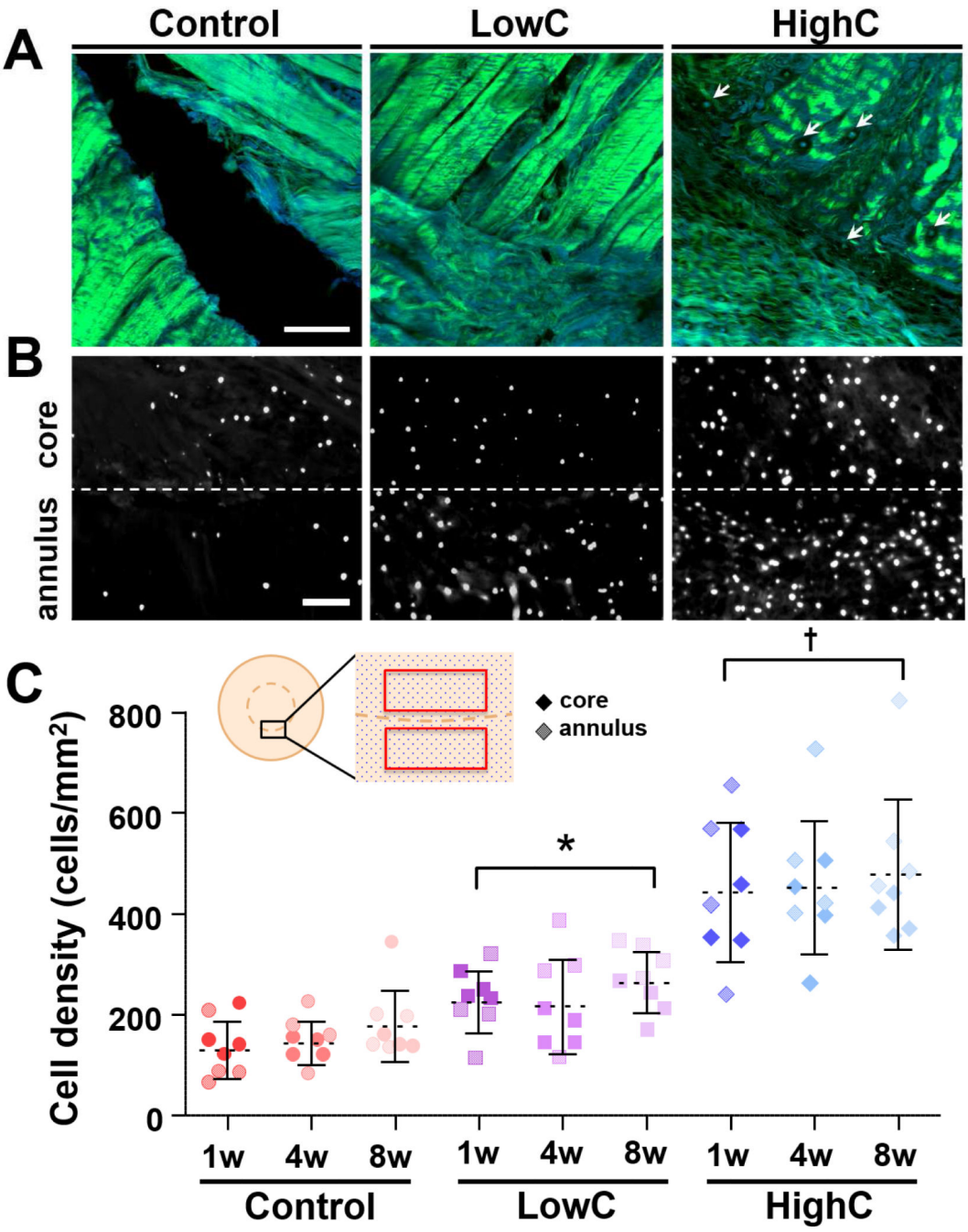

Figure 2. Degradation of the wound interface reduces matrix density and increases cellularity in an *in vitro* meniscal repair model

(A) Second harmonic generation imaging shows collagen fibers (green) at the wound interface of control, low-dose collagenase (LowC; 0.01 mg/mL), and high-dose collagenase (HighC; 0.05 mg/mL) repair constructs after 1 week of *in vitro* culture. Blue indicates autofluorescent signal. Arrows point to cells within the matrix. Scale = 100 μm. (B) DAPI staining of axial sections show cell nuclei at the interface (dashed line) after 1 week. Scale = 100 μm. (C) Cell density at the interface with respect to treatment group and *in vitro* culture time (n = 4 samples/group, mean ± standard deviation). Cores (dark) and annuli (light) were

counted as independent data points (no statistical difference). Inset shows schematic of repair explant in an axial section, where the boxes highlight the cell counting regions. ***** = $p \leq 0.05$ vs. Control. † = $p \leq 0.05$ vs. Control and LowC. There was no difference between time points within the same treatment group.

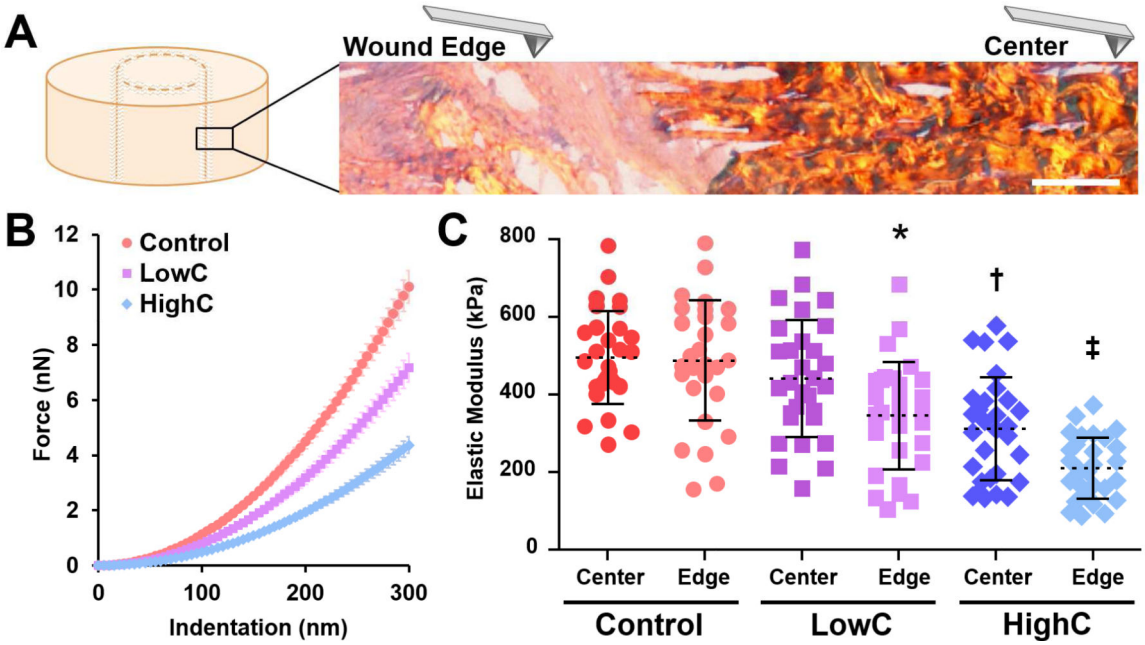

Figure 3. Location-dependent matrix micromechanics of repair constructs after 8 weeks of *in vitro* culture

(A) Schematic of AFM nanoindentation measurements of matrix stiffness across the wound interface of a HighC construct stained with PSR (collagen). Scale = 50 μm. (B) Force indentation curves for each condition taken at the wound edge (mean ± standard error of the mean for all samples). (C) Elastic modulus of the construct center and wound edge of Control, LowC, and HighC constructs (n = 3 samples/group, 10 measurements/sample, mean ± standard deviation). * = $p \leq 0.05$ vs. Control. † = $p \leq 0.05$ vs. Control and LowC. ‡ = $p \leq 0.05$ vs. all other groups.

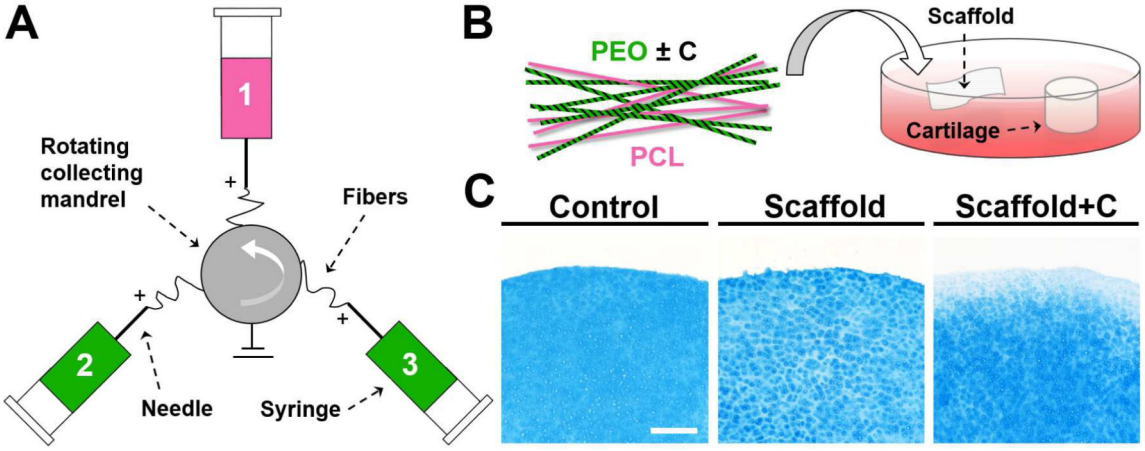

Figure 4. Fabrication of composite nanofibrous scaffolds with and without collagenase

(A) Schematic of tri-jet electrospinning. (B) Schematic of composite scaffold composed of poly(ε-caprolactone) (PCL) and poly(ethylene oxide) (PEO) fiber fractions, where enzyme activity was localized to soluble PEO fibers. Bioactivity was verified by incubation with cartilage cylinders. (C) AB staining of cartilage after 72 hours in Control, Scaffold, and Scaffold+C groups. Staining intensity decreased at the tissue edge, indicating bioactivity of the released collagenase. Scale = 250 μm.

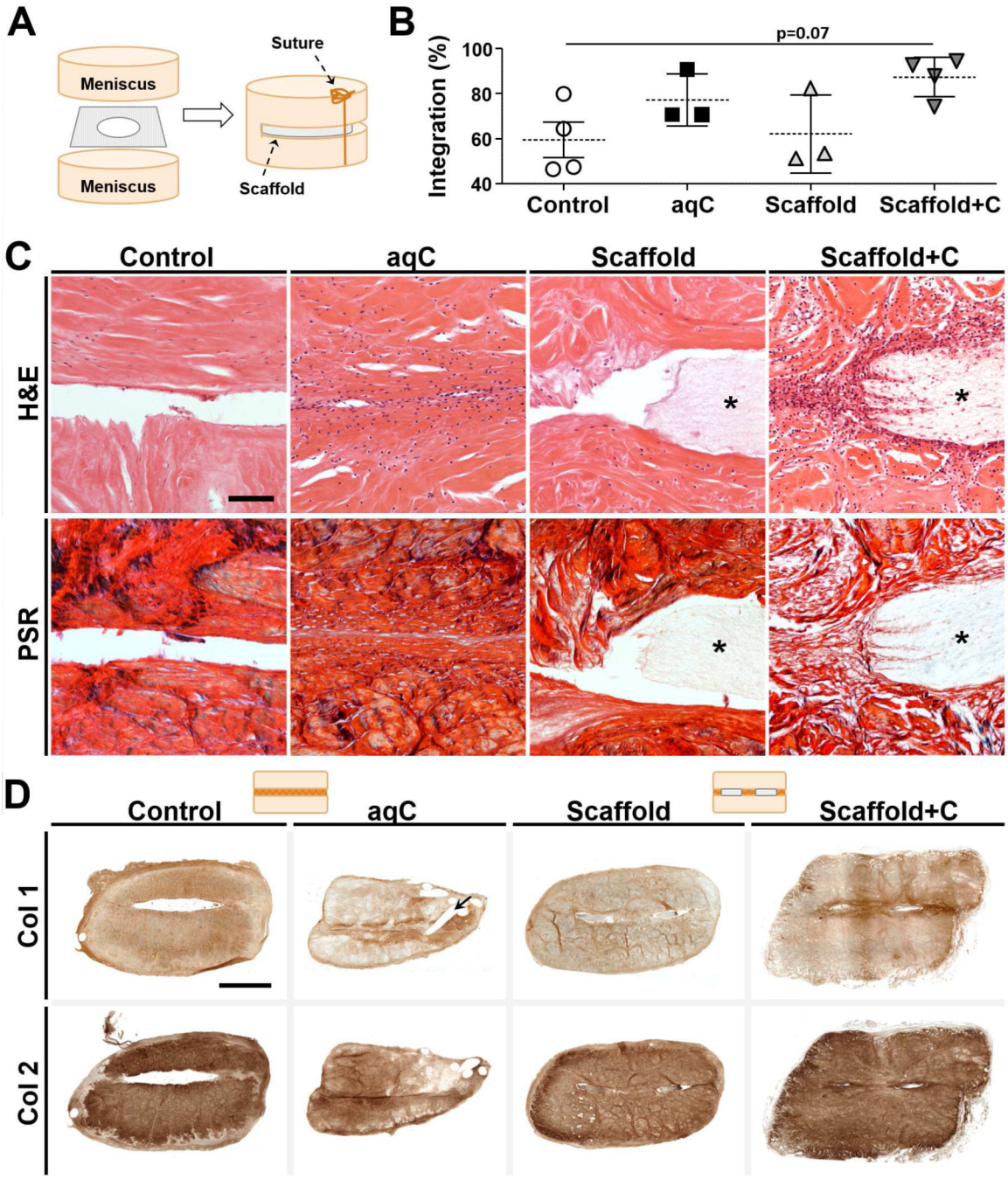

Figure 5. Collagenase treatment improves meniscal integration after 4 weeks of subcutaneous implantation

(A) Schematic of repair construct assembly. Scaffold is fenestrated to allow tissue-to-tissue contact. (B) Quantification of histological integration normalized to defect length (n = 3-4 samples/group, mean ± standard deviation). Line indicates trend for difference between groups (p = 0.07). (C) H&E (cells and matrix) and PSR (collagen) staining at the defect site after 4 weeks. Asterisk indicates scaffold. Scale = 100 μm. (D) Immunohistochemistry for type I and II collagen. Staining at interface was of higher intensity for collagenase-treated groups (aqC and Scaffold+C), and largely absent in Control and Scaffold groups. Arrow

indicates suture track in aqC sample. Schematic illustrates transverse cross-section with or without fenestrated scaffold present. Scale = 2 mm.

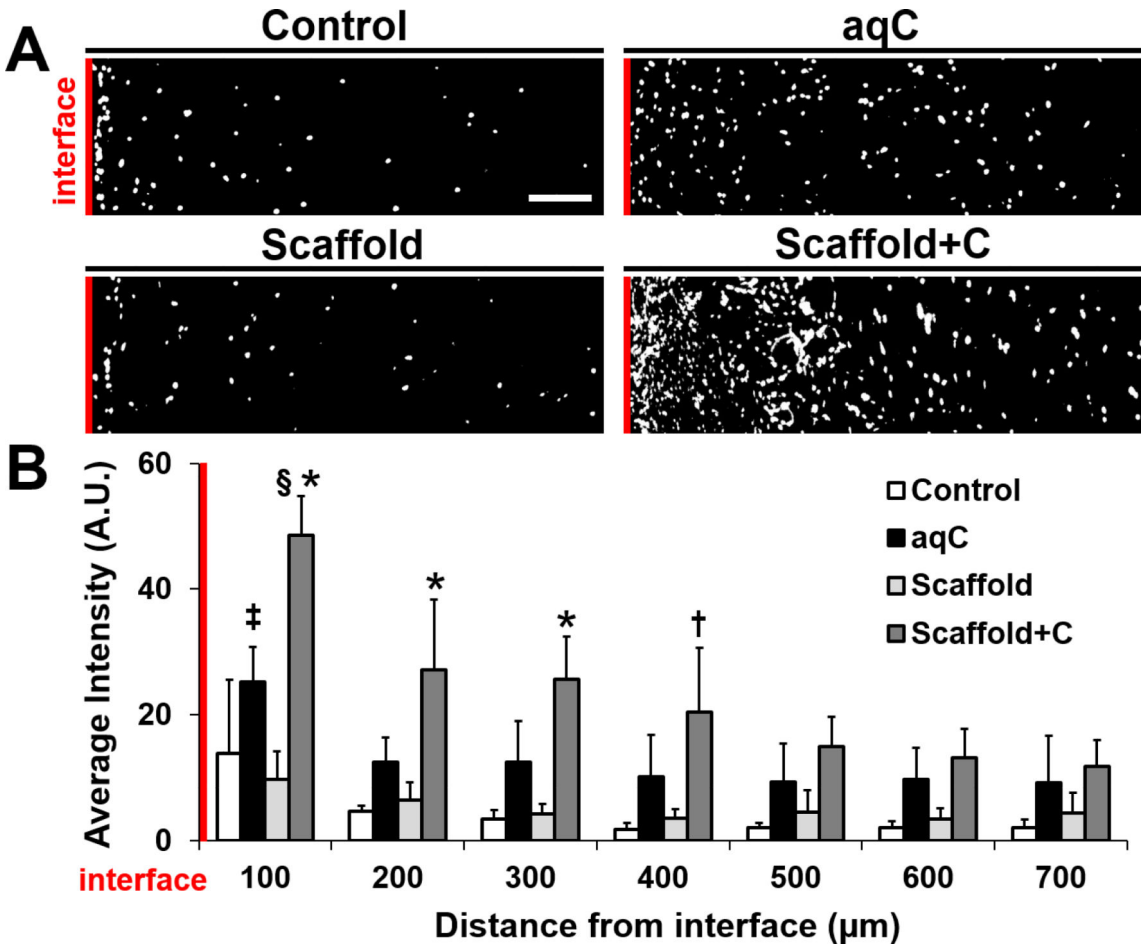

Figure 6. Cellularity proximal to the wound interface increases with collagenase treatment after 4 weeks of subcutaneous implantation

(A) Thresholded images of DAPI-stained nuclei for each group at 4 weeks. Interface is on the left (red line). Scale = 100 μm. (B) Average intensity with respect to distance from the interface (n = 4/group, mean ± standard deviation). * = $p \leq 0.05$ vs. all other groups at the same distance, † = $p \leq 0.05$ vs. Control and Scaffold at the same distance, ‡ = $p \leq 0.05$ vs. aqC distances ≥ 400 μm, § = $p \leq 0.05$ vs. all other Scaffold+C distances.

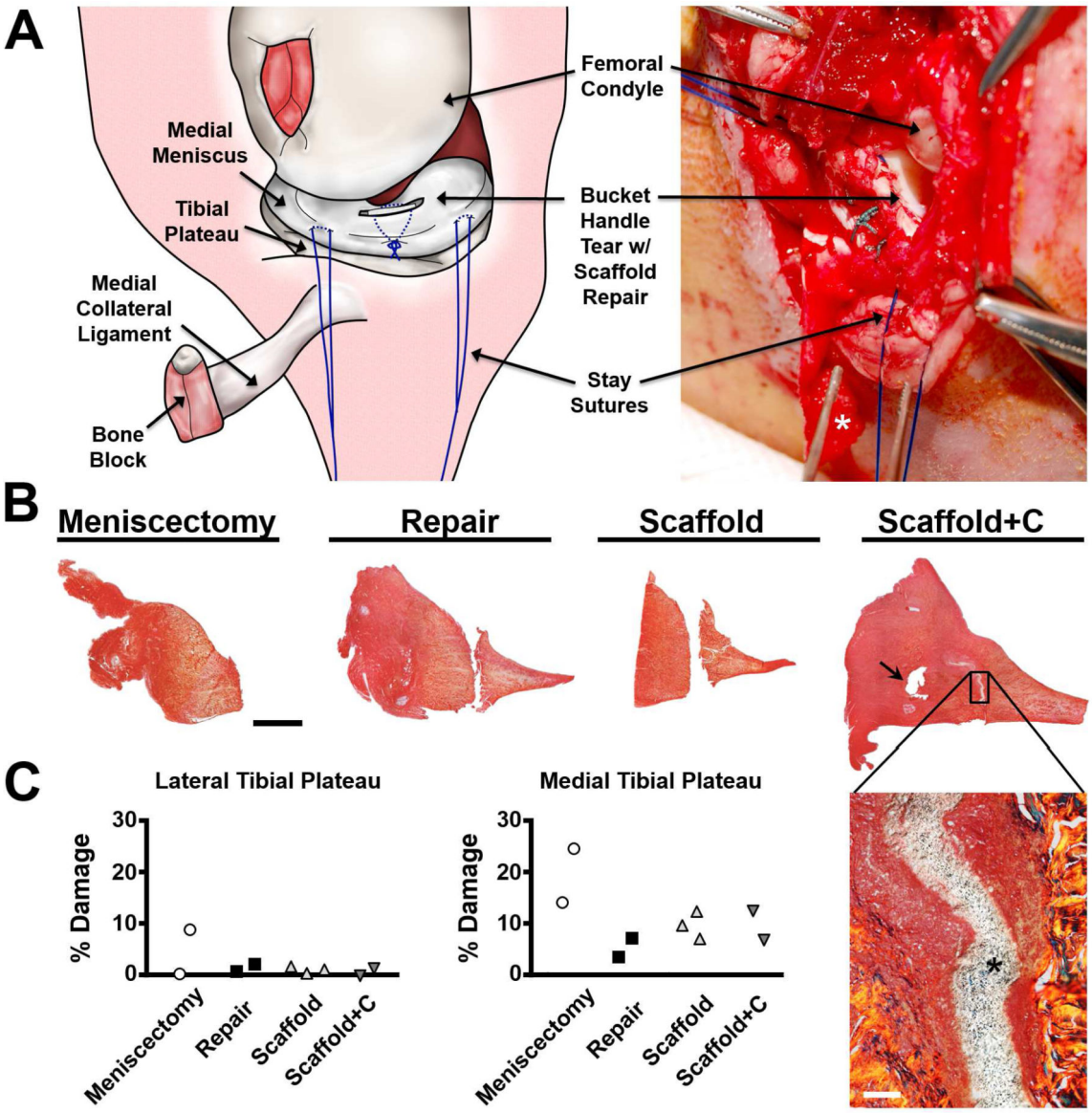

Figure 7. Collagenase-releasing scaffolds promote repair at 4 weeks in an ovine meniscal defect model

(A) Schematic and photograph of surgical approach, longitudinal meniscal injury, and suture repair with scaffold. Asterisk indicates the bone block. (B) Radial sections of the repaired meniscus at 4 weeks, stained with PSR (collagen). Arrow indicates suture track. Scale = 2 mm. Magnified area shows enhanced integration of Scaffold+C with adjacent tissue, where the asterisk indicates the scaffold. Scale = 100 μm. (C) Quantification of damage to cartilage using India ink. Collagenase release by Scaffold+C did not adversely affect the cartilage.

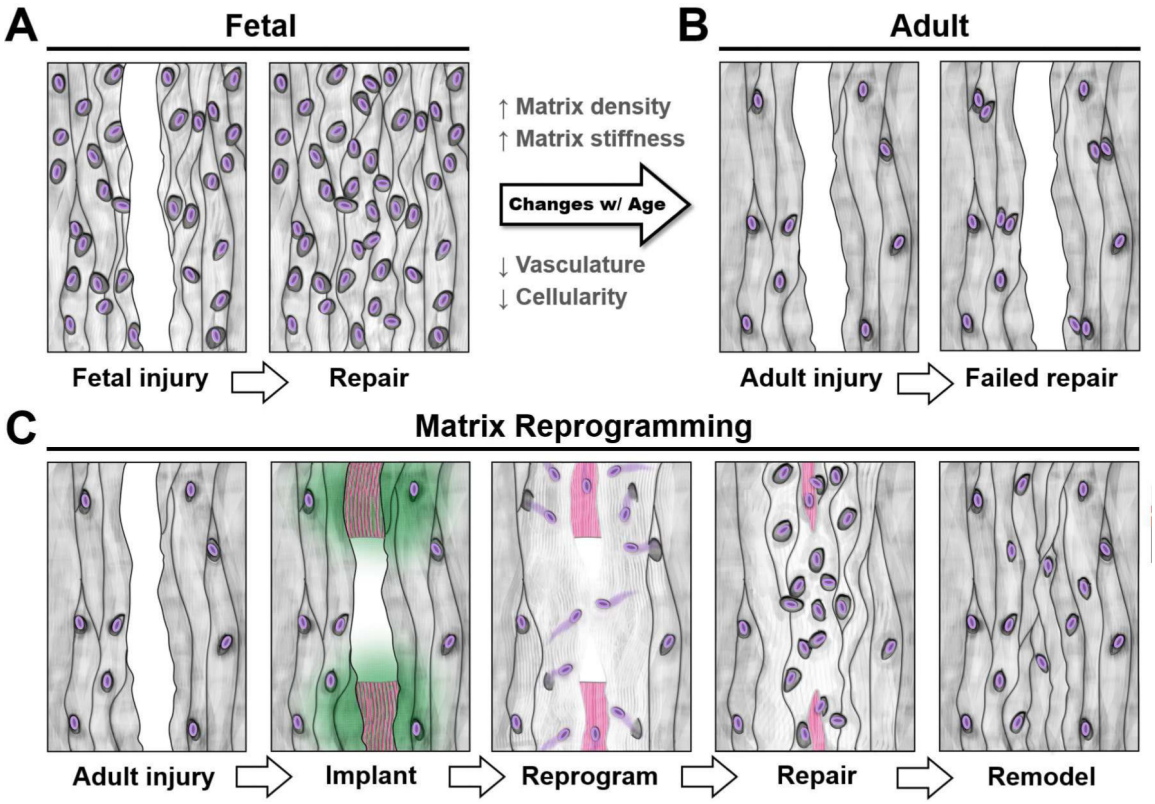

Figure 8. Extracellular matrix reprogramming of the wound interface to a fetal-like state augments dense connective tissue repair

(A) Injury to fetal tissue results in a rapid repair, with cells rapidly colonizing the wound site and depositing new matrix. (B) Conversely, healing of adult tissue is limited because few cells arrive at the wound site. (C) Scaffold-mediated reprogramming via collagenase-releasing nanofibers (green) reduces local matrix stiffness and density, thereby releasing cells from these steric constraints. The wound gap is bridged as cells colonize the defect and deposit matrix around the remaining scaffold (pink). Over time, the scaffold degrades, allowing cells to remodel the interface.